Nuclear Inst. and Methods in Physics Research, A 986 (2021) 164814

Contents lists available at ScienceDirect

Nuclear Inst. and Methods in Physics Research, A

journal homepage: www.elsevier.com/locate/nima

Study of the radiation-induced damage mechanism in proton irradiated low gain avalanche detectors and its thermal annealing dependence

Moritz Wiehe [a,b,*], Marcos Fernández García [a,c], Salvador Hidalgo [e], Michael Moll [a], Sofia Otero Ugobono [a,d], Ulrich Parzefall [b], Giulio Pellegrini [e], Ana Ventura Barroso [a,f], Ivan Vila Alvarez [c]

[a] CERN, Route du Meyrin 285, CH-1211 Genève 23, Switzerland
[b] Albert-Ludwigs-Universität Freiburg, Physikalisches Institut, Hermann-Herder-Str. 3, 79104 Freiburg, Germany
[c] Instituto de Física de Cantabria (CSIC-UC), Avda. los Castros s/n, E-39005 Santander, Spain
[d] Universidade de Santiago de Compostela, Santiago de Compostela, A Coruña, Spain
[e] Instituto de Microelectrónica de Barcelona (IMB-CNM-CSIC), Barcelona, Spain
[f] University of Barcelona, Gran Via de les Corts Catalanes 585, 08007 Barcelona, Spain

ARTICLE INFO

Keywords:
Silicon sensors
Avalanche multiplication
Radiation hardness
High irradiation environment

ABSTRACT

In this study the effects of proton irradiation and annealing on Low Gain Avalanche Detectors (LGADs) are investigated. Two LGADs and one p-in-n diode, produced by CNM (Centre Nacional de Microelectrònica 2018), were irradiated with 24 GeV/c-protons to a fluence of 1×10^{14} n_{eq}/cm^2 and annealed at 60 °C for up to 5000 min. The sensors have an active area of 3×3 mm^2 and a thickness of 277 μm. Current– and capacitance–voltage measurements, as well as laser measurements using the transient-current-technique were carried out to study the change of gain and the electric field after irradiation and consecutive annealing steps. The reduction of gain after irradiation is the main concern when using LGADs in high energy physics experiments. After annealing the sensors, no recovery of gain was observed. Different ways to measure the gain layer depletion voltage are discussed.

1. Introduction

Ever increasing particle energies and track densities in modern high energy particle physics experiments pose high demands on the radiation hardness of detector systems. With the High Luminosity upgrade of the Large Hadron Collider, the integrated luminosity will increase by about a factor of 10 and the radiation doses will be as high as 10^{16} n_{eq}/cm^2. For future hadron collider projects these numbers will be significantly higher. For high luminosity environments, sensors for timing applications become more and more important: Due to the higher number of particle interactions, disentangling primary vertices purely by spatial track measurements becomes increasingly challenging. Resolving different particle interactions also in time will help to reconstruct tracks and assign them to the correct primary vertex. The two main factors limiting the timing resolution are time jitter and Landau noise [1]. Where as the Landau noise, resulting from fluctuations in deposited charge, cannot be avoided, the time jitter can be reduced by increasing the signal slew rate while maintaining the same noise level. To maintain a good signal-to-noise ratio and to decrease the signal rise time, sensors with intrinsic gain have been developed [2–5]. The increase of signal charge is obtained by exploiting the effect of avalanche multiplication of drifting charge carriers in a high electric field. Plans to include silicon detectors designed for timing applications exist for example for the ATLAS High Granularity Timing Detector [6], the CMS MIP Timing Detector [7], the CMS/TOTEM Precision Proton Spectrometer [8] or the LHCb detector [9]. Low Gain Avalanche Detectors (LGADs, [10]) are based on the technology of Avalanche Photodiodes (APD) [11] but are designed to have a lower gain value for increased temperature and voltage stability, lower fluctuations in signal amplitude and to allow for finer segmented sensors [2]. LGADs have a heavily n-doped read-out electrode and a thin (several µm) p-doped multiplication layer directly beneath it. The electric field at the junction is high enough for charge multiplication to occur. Read-out and multiplication layers are implanted in a p-type bulk. The gain of the device is defined by the doping profile and doping concentration of the multiplication layer.

To develop detectors for applications in high energy physics experiments a good understanding of the radiation damage mechanisms is crucial. Tests of LGADs revealed that the gain of the device is heavily degraded after irradiation with highly energetic particles, which is detrimental for operation [12,13]. It is known that the gain is more

* Corresponding author at: CERN, Route du Meyrin 285, CH-1211 Genève 23, Switzerland.
E-mail address: m.wiehe@cern.ch (M. Wiehe).

https://doi.org/10.1016/j.nima.2020.164814
Received 23 June 2020; Received in revised form 29 September 2020; Accepted 21 October 2020
Available online 24 October 2020
0168-9002/'

heavily reduced after irradiation with charged hadrons compared to neutrons [14]. A prominent way of explaining the reduction of gain after irradiation is the effect of acceptor removal [15–17]. A proposed reason for this is that boron dopants can be removed from their position in the silicon lattice inside the multiplication layer by impinging high energy particles. The dislocated boron atom can then form a defect complex with an oxygen interstitial (B_iO_i) and is thus electrically deactivated [16,18,19]. By this process the effective doping concentration of the multiplication layer is reduced. This leads to a lower electric field at the junction and reduces the amount of multiplied charge. On the other hand, device simulations of radiation damage after proton irradiation on LGADs, even without implementation of the acceptor removal process, show a decrease in electric field strength, and therefore a reduction of gain, at the multiplication implant [20]. The radiation effects are explained by solely modeling two effective (donor/acceptor) trap levels and the predominant trapping of holes produced in the multiplication process. The reduction of the electric field at the multiplication implant is accompanied by the build up of an electric field region at the backside of the sensor (double junction) and a reduced electric field in the middle of the device and directly below the multiplication implant. The effective space charge is affected both in the multiplication implant and the sensor bulk, which becomes effectively n-type. In a similar approach, taking acceptor removal into account, the agreement with experimental data can be improved [21].

LGADs have been tested with respect to their charge collection capabilities after irradiation with reactor neutrons, 192 MeV pions and 800 MeV protons [13]. The proposed method [13] for measuring the bias voltage at which the multiplication layer is depleted is to inject charge in a volume close to the multiplication layer (e.g. using a red laser). Due to the very limited drift length of the charge carriers in the non-depleted multiplication layer, no signal is detectable. Only if the multiplication layer is depleted and the depleted region starts to extend into the sensor bulk, the charge carriers can drift over a large enough distance to create a current signal. The injection of red light to the top side of the detector (location of the multiplication layer) showed that the depletion voltage of the multiplication layer decreases with fluence. This effect was explained by effective acceptor removal in the multiplication layer, which leads to a reduced depletion voltage of the p^+-layer. The compensation of space charge within the multiplication layer due to the build-up of positive space charge introduced by radiation induced defects, was excluded from being the main reason by the exponential decrease of the depletion voltage of the multiplication layer. The amount of reduction depends on the type of particle used for irradiation and was found to be in agreement with the expected gain reduction after hadron and neutron irradiation. Also, the effect was observed to be independent from temperature and free carrier concentration, which further supports the explanation by initial acceptor removal.

In contrast to the aforementioned results, an increase of depletion voltage of the multiplication layer was observed with higher irradiation, using 24 GeV/c-protons [22]. The effect was related to the formation of a double junction, which can be explained by increased positive space charge, i.e. increased occupancy of defects with holes, at the backside of the device, eventually leading to a positive space charge region in the bulk of an irradiated p-type sensor [23,24]. Using backside-illumination, it was observed that already at low voltages an electric field develops at the rear of the devices. The decrease in overall gain was attributed to both the formation of a double junction and the aforementioned acceptor removal.

In the study presented here, irradiated LGADs are investigated using the Transient Current Technique (TCT) [25] as well as current–voltage (IV) and capacitance–voltage (CV) measurements. The sensors were irradiated to a fluence of 10^{14} n_{eq}/cm^2 using 24 GeV/c-protons. To further investigate the effect of irradiation on LGAD devices an annealing study was performed. For annealing times ranging from 80 to about 5000 min at 60 °C, the collected charge, the gain and the electric field profile is measured.

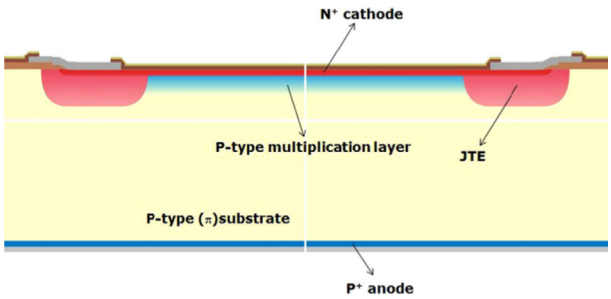

Fig. 1. Schematic cross-section of the LGAD pad design with a JTE structure protecting the junction edge termination [10].

2. Experimental method

2.1. Samples

Two LGADs and one p-in-n (PIN) diode were used for this study (LGADs: W5_E3_1, W5_I3_1, PIN: W5_E3_4). All three samples were produced by CNM [26] in run 8622 and are originating from the same wafer (W5). The LGADs have a medium dose multiplication implant directly beneath the top read-out electrode and a Junction Termination Extension (JTE) [10]. A schematic drawing is shown in Fig. 1. The JTE is used to obtain a more homogeneous electric field profile along the edge of the multiplication implant, to increase gain homogeneity and high voltage stability. All sensors are equipped with a guard ring. The PIN diode is identical to the LGADs except for the fact that it does not have an multiplication layer. Therefore, the PIN diode served as a reference sensor, to identify effects related to the multiplication layer. All sensors have an active area of 3×3 mm^2 and a thickness of 277 µm. The samples were irradiated at the CERN IRRAD facility [27,28] to a fluence of 1×10^{14} n_{eq}/cm^2 using protons with an energy of 24 GeV/c. The 1 MeV neutron equivalent fluence was calculated using a hardness factor of $\kappa = 0.62$. Before irradiation the depletion voltage, obtained from CV measurements, of the LGADs and the PIN diode was 70 V and 40 V respectively. The current at full depletion ranges from 30 nA for the PIN diode to 60–90 nA for the LGADs at room temperature.

2.2. Experimental setup

For this study TCT and edge-TCT as well as IV and CV measurements were performed. TCT and edge-TCT measurements were carried out on the TCT+ setup of the SSD laboratory at CERN [29]. The response of the sample can be measured using infrared (1064 nm) or red (660 nm) laser pulses which can be injected from the front or back side of the sample, as well as from the edge for infrared light. The devices under test (DUTs) are glued to a printed circuit board (PCB) which is equipped with SMA-connectors for the bias voltage supply, read-out and optional guard-ring connection. The glue is conductive and establishes the back side connection. The read-out electrode and guard ring on the front side of the sensor are connected to the PCB with wire-bonds. A PT1000 temperature sensor is attached to the PCB close to the DUT. To facilitate measurements from the back side or the edge, the PCBs feature holes and cut-outs for the laser. The PCB is mounted on a copper plate, which is cooled by a Peltier element. The heat is removed from the setup with a Huber CC505 chiller. The minimum reachable temperature of the setup, depending on the sample and its power dissipation, is about −25 °C. The sample holder is mounted on a Newport three-axis linear stage system. The stages have a stepping resolution of 300 nm in x and y and 100 nm in the z direction. Stage system and laser optics are contained in a Faraday-cage for electro-magnetic isolation. To avoid condensation, the whole cage is flushed with dry air. For light generation, two PicoQuant lasers with a pulse length of 200 ps are used. The light is guided to the objectives using optical fibers. The DUT signal

is amplified by a Cividec 2 GHz/40 dB amplifier and displayed on an Agilent Technologies DSO9254A digital oscilloscope. To monitor the power of the laser, part of the beam is directed onto a reference diode. Its signal is recorded with the DUT data and used in the analysis to normalize the signal to account for fluctuations in the laser output. Most components of the setup are controlled by a LabView software. After mounting the sample and setting up the measurement parameters, the measurement is performed automatically and the data is saved to disk.

For IV and CV measurements a Binder MKT115 climate chamber is used for cooling the sensors. Current and capacitance are measured with a Keithley 6487 picoammeter and a Keysight E4980A LCR-meter. For measurements in the climate chamber the DUTs remain on the same PCB as for TCT measurements.

For annealing, the samples/PCBs are put in an oven at 60 °C for the respective amount of time.

2.3. Measurements

TCT measurements, illuminating the sample from the top surface using a red laser (RF-TCT), were performed at −20 °C and +20 °C. Edge-TCT (eTCT) measurements were only performed at −20 °C. For RF-TCT measurements a spot in the middle of the opening in the top metallization of the DUT was used for light injection. For a fixed laser position the bias voltage was ramped from 0 to 400 V in 2 V steps. For eTCT measurements a voltage range from 0 to 300 V, in 5 or 10 V steps was used. In addition, the laser beam position along the sensor edge (z-axis) was varied in 2 or 3 μm steps. For each point the oscilloscope averages over 256 individual waveforms. The sensor was biased from the backside and the signal was read out from the top electrode at ground potential. The guard ring was connected to ground over a 50 Ω resistor. RF-TCT measurements before irradiation were performed with the signal read out at the backside. All recorded signals are normalized to the same laser power, using the reference diode, as described in Section 2.2. For measurements of the collected charge, the signal was integrated for 25 ns.

IV and CV measurements are performed at −20 °C. The guard ring was left floating for these measurements for technical reasons. The capacitance was measured in parallel mode at a frequency of 10 kHz and a signal amplitude of 0.5 V. The bias voltage was varied from 0 to 400 V.

The samples were measured before irradiation and after 80 min of annealing at 60 °C after irradiation. After this, all measurements were repeated after consecutive steps of increasing annealing time.

3. Results

3.1. Gain

It is possible to calculate the signal gain due to multiplication in different ways. One way is to measure the response of an LGAD to top and backside illumination. A comparison of the respective integrated signals allows to calculate the gain of the device. A second way is to compare the TCT measurements with top injection after full depletion of an LGAD to those of a PIN-diode with the same design parameters, except for the multiplication layer. In this study the value is obtained by the latter method only. For this, measurements of an LGAD and the PIN diode at the same annealing state are compared. For both devices, the collected charge as a function of bias voltage is calculated individually, by integrating the current signal for 25 ns. The gain is then calculated by

$$Gain(V) = \frac{Q^{LGAD}_{25ns}(V)}{Q^{PIN}_{25ns}(V)}. \quad (1)$$

In Fig. 2 the gain at a bias voltage of 400 V is shown as a function of annealing time for both LGADs for measurements at −20 °C and +20 °C.

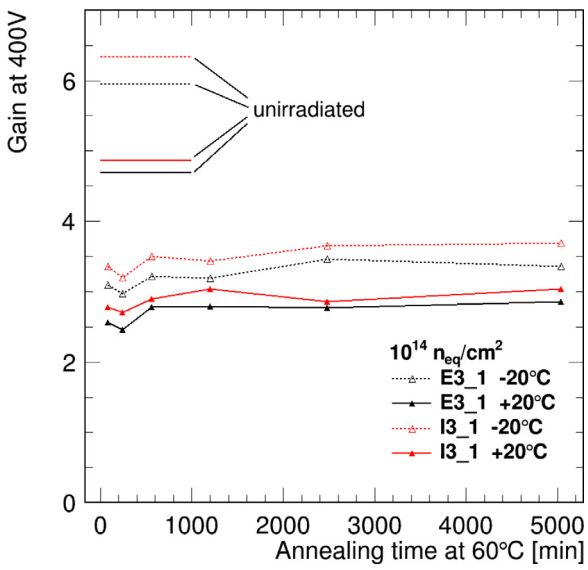

Fig. 2. Charge gain at 400 V as a function of annealing time at 60 °C. The gain is calculated using RF-TCT measurements, comparing the PIN diode and the LGADs in the same annealing state. Measurements before irradiation are shown as horizontal lines.

The values before irradiation are shown as a horizontal line at the left side of the plot. Before irradiation the gain is around 4.5 and 6 for measurements at +20 °C and −20 °C, respectively. The different gain values for different temperatures can be explained by the temperature dependence of the impact ionization coefficient in silicon. The relative decrease in gain of about 20%–25% with an increase in temperature of 40 °C is comparable to observed and simulated values in literature [30,31]. The sensor named W5_E3_1, depicted in black, has a slightly lower gain before as well as after irradiation and annealing. After irradiation the gain is reduced to values ranging from 2.5 to 3.5. This corresponds to a relative decrease in gain of about 40 to 45%. This reduction of gain can be compared to other studies, where the gain almost completely vanished after charged hadron irradiation of LGADs to a fluence of 5×10^{14} n_{eq}/cm^2 [13]. As pointed out earlier, the reduction of gain due to irradiation can be explained by a combination of acceptor removal and a redistribution of the electric field due to charged defects. The measurements presented here show that the amount of gain does not change with annealing. A process which is believed to be significantly contributing to acceptor removal is the formation of B_iO_i defect levels, effectively deactivating the implanted boron. Also thermally stimulated current (TSC) measurements reveal that this defect level is not affected by annealing [19].

3.2. Leakage current

Measurements of the leakage current of LGADs, or similarly of APDs, show a distinct shape which is caused by the different doping concentrations of the sensor bulk and the multiplication layer [11,32]. The charge multiplication in LGADs is a consequence of impact ionization, which depends mainly on the local electric field [33,34]. At low reverse bias voltages the multiplication layer starts to deplete well before the electric field extends into the sensor bulk. Due to the strong doping of the gain layer, the increase in voltage mainly causes an increase of electric field strength in the multiplication layer while the increase in depletion width is minimal. Once the multiplication layer is depleted, the depleted volume quickly extends into the sensor bulk, giving rise to a sharp increase of the leakage current. An increase in bias voltage after the multiplication layer is depleted will lead to an enlarged depleted volume in the bulk and eventually to an increased electric field over the whole detector.

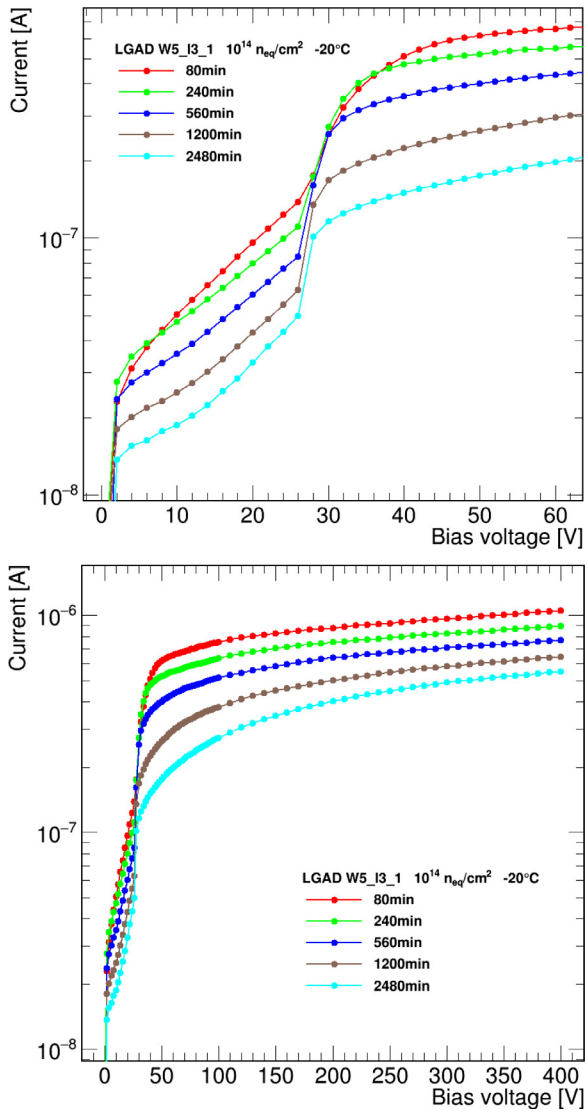

Fig. 3. Leakage current of LGAD W5_I3_1 as a function of bias voltage at −20 °C for different annealing times. The data is shown in a limited voltage range (top) and in the full range (bottom).

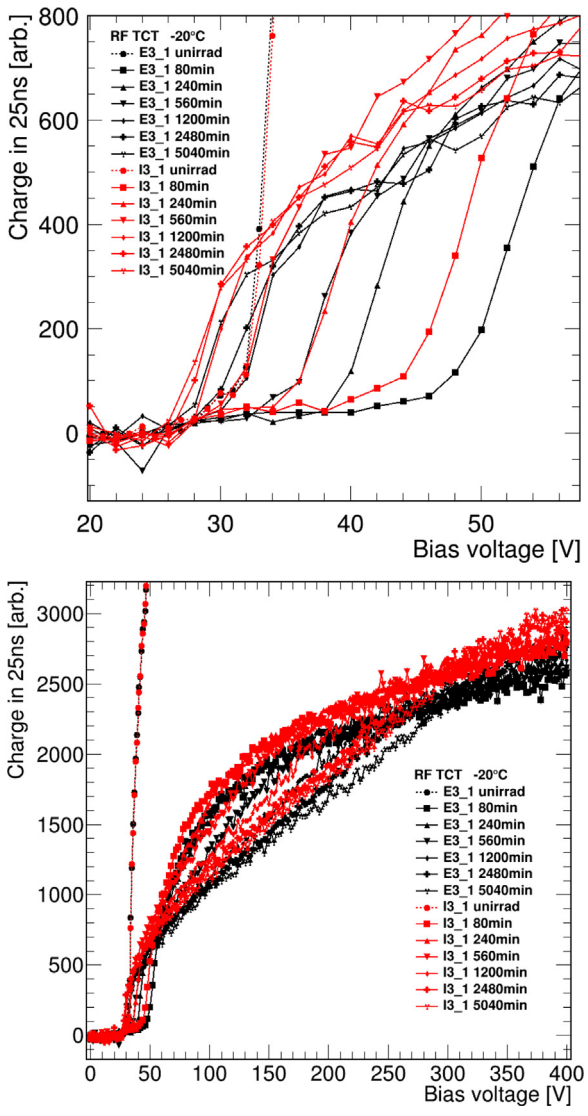

Fig. 4. Collected Charge in 25 ns with RF-TCT as a function of bias voltage for both LGADs, depicted in red and black, at different annealing times. The shown measurements were performed at −20 °C. Measurements before irradiation are depicted as dashed lines. The data is shown in a limited voltage range (top) and in the full range (bottom).

In Fig. 3 the leakage current measured at −20 °C is shown for LGAD W5_I3_1 for different annealing times. No temperature scaling is applied in this figure. As expected, the leakage current decreases with increasing annealing time (see also Fig. 11). As described above, two distinct trends can be identified in the leakage current measurements: (1) Because of the relation of impact ionization and electric field strength the increase of the leakage current for voltages below the depletion of the gain layer roughly follows an exponential trend. It was verified that this exponential increase in current at low voltages is a result of multiplication in the gain layer by performing IV measurements on unirradiated LGADs and PINs of the same production run with different gain layer doping concentrations while continuously illuminating the devices with a red LED during the measurement. (2) At 26 V an abrupt increase of leakage current is observed. The position of the kink is independent of annealing time. It can be assumed that at this voltage, the electric field extends into the bulk, quickly increasing the depleted volume and therefore the leakage current. The second LGAD shows the same behavior, again at 26 V for all annealing times. The amount of impact ionization increases less quickly after depletion of the gain layer and the increase in current is mainly caused by the increase of depletion width. In the top figure the focus is on the leakage current behavior at low voltages. The current was measured to up to 400 V (bottom figure). No breakdown of any of the devices was observed during the measurements. Under the assumption, that the sensor bulk only depletes once the gain layer is fully depleted, the leakage current measurements indicate a gain layer depletion voltage of $V_{mr} = 26$ V.

3.3. TCT - onset voltage

The value of the bias voltage at which a sharp increase in induced charge is observed after charge injection by red laser light to the top side of an LGAD (RF-TCT) is called onset voltage in the following. In Fig. 4 the collected charge in 25 ns as a function of bias voltage is shown for both LGADs, measured at −20 °C. Measurements before irradiation are shown with a dashed line. The two LGADs, depicted in red and black, show the same behavior qualitatively: Nearly no signal can be seen up to a certain point from where on the signal rises abruptly. The bias voltage needed for a signal to be measured varies with annealing time. The value of the onset voltage is determined by a fit to the

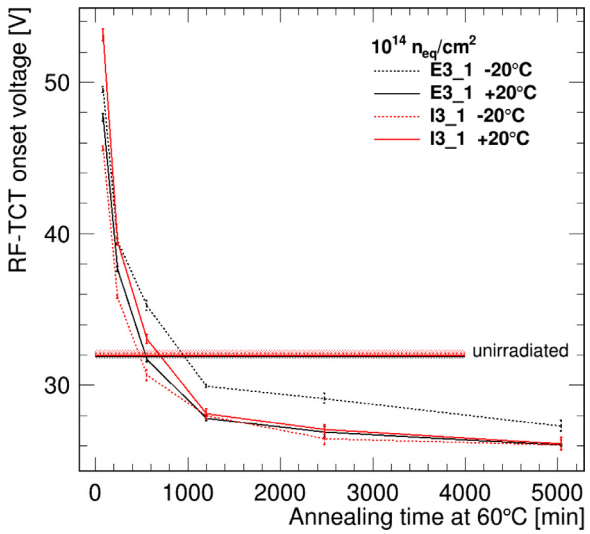

Fig. 5. Onset voltage as a function of annealing time. Both LGADs at temperatures of −20 °C and +20 °C are shown. The measurements before irradiation are depicted as horizontal lines.

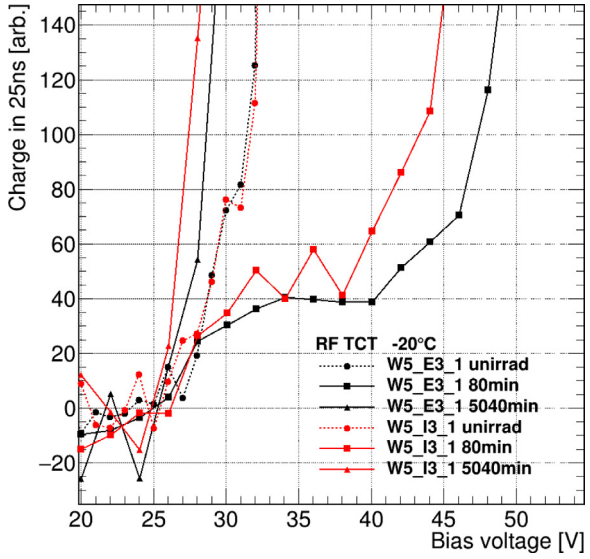

Fig. 6. Collected Charge in 25 ns as a function of bias voltage for both LGADs before irradiation and after 80 and 5040 min of annealing. Measurements were performed at −20 °C. The measurements before irradiation are depicted as dashed lines.

collected charge with

$$Q_{25\ \mathrm{ns}} \propto \begin{cases} \sqrt{V_{bias} - V_{onset}} & \text{for} \quad V_{bias} \geq V_{onset} \\ 0 & \text{for} \quad V_{bias} < V_{onset} \end{cases} \tag{2}$$

The obtained values of the onset voltage are shown in Fig. 5 as a function of annealing time for the two LGADs, measured at −20 °C and +20 °C. No systematic dependence on temperature is observed. The onset voltage before irradiation (horizontal line) is about 32 V. After irradiation the same measurement results in values of 45 to 50 V for both devices. With increasing annealing time the onset voltage is reduced to values around 26 V. This last value coincides with the gain layer depletion voltage which was extracted from measurements of the leakage current (Fig. 3).

Before the signal onset voltage is reached, especially for low annealing times, the collected charge is not exactly zero. Rather two distinct steps in the measured signal charge can be observed: One at a fixed voltage of around 26 V, followed by the onset voltage discussed above.

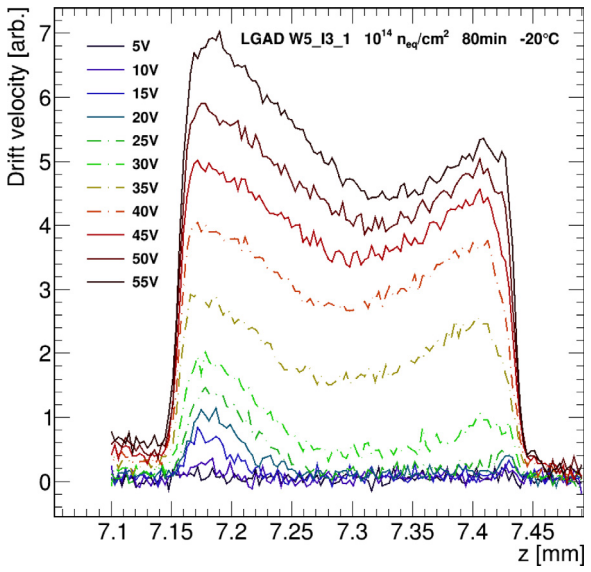

Fig. 7. Drift velocity for LGAD W5_I3_1 as a function of sensor depth for different bias voltages, measured after 80 min of annealing at 60 °C. The front side of the sensor (position of the multiplication layer) corresponds to the position $z \approx 7.15$ mm.

Fig. 6 shows the exact same data as Fig. 4 but is plotted on a smaller scale. It can be seen that two separate processes lead to the increase of the signal charge at different voltages. The plateau between 25 and 40 V for the measurement after 80 min of annealing is not described by Eq. (2).

3.4. Electric field

To better understand the influence of irradiation and annealing on the electric field inside an LGAD, edge-TCT measurements were carried out. The drift velocity of the charge carriers is calculated by integrating the first 600 ps of the measured signal. From the relation between the signal current, drift velocity and electric field and under the assumption of a constant charge carrier mobility μ, it is possible to estimate the shape of the electric field [35]:

$$I(t \approx 0) \propto v_{drift} \propto \mu(E)E(z) \tag{3}$$

In Fig. 7 the drift velocity, at a temperature of −20 °C, is shown as a function of the beam position in LGAD W5_I3_1 for different bias voltages. Here only results for one sensor are shown, the second LGAD shows the same behavior. The measurement was performed after irradiation and 80 min of annealing. The left hand side of the plot (at $z \approx 7.15$ mm) corresponds to the front side (location of the multiplication layer) of the device. For voltages below 30 V, before the gain layer is depleted, a non-zero drift velocity can be observed at a narrow region towards the multiplication layer. This effect is also visible in measurements before irradiation and might be attributed to the non-homogeneous doping profile, charges diffusing into the gain region and the widening of the laser beam traversing the silicon sensor. More remarkably, it can be seen that, increasing the bias voltage from 25 V to 30 V, the measurement yields non-zero values across the whole sensor bulk. This increase in signal throughout the bulk is observed as well for annealing times of 240 and 560 min at the same voltages. The measurements of the unirradiated sensor show a significant signal increase at higher voltages of about 35 V to 40 V. Additionally one can see that for low bias voltages the electric field is higher at the backside of the device, with a lower electric field strength in the middle of the sensor. This behavior is usually referred to as a double junction. For longer annealing times this effect is not visible anymore, as can be seen in Fig. 8: The drift velocity profile is shown for only one bias

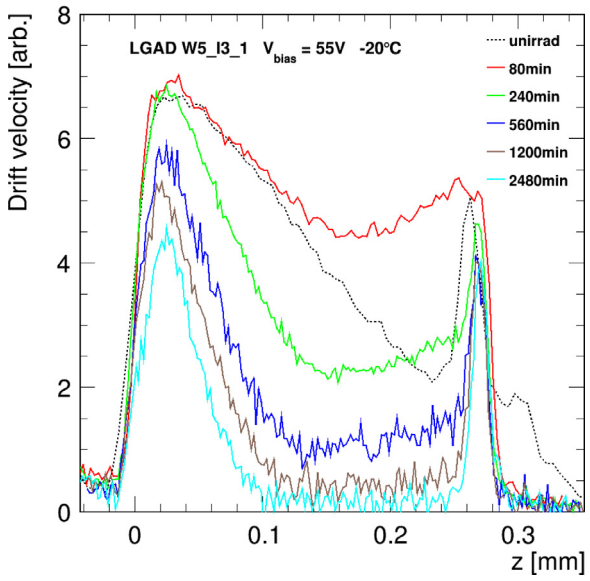

Fig. 8. Drift velocity for LGAD W5_I3_1 as a function of sensor depth for different annealing times, measured at a bias voltage of 55 V. The front side of the sensor (position of the multiplication layer) corresponds to the position $z = 0$. The reference point on the horizontal axis to overlay the individual measurements is arbitrary.

voltage (55 V) for the different annealing times. Here it is evident that after 80, 240 and 560 min of annealing the electric field is higher towards the backside of the device. With progressive annealing time the double junction effect vanishes and the electric field seems to be more confined to the front side of the sensor. The measurement of the unirradiated device shows a linearly decreasing field towards the rear side, which extends throughout the full detector bulk. The narrow peak at the backside of the device originates from the difference of doping concentration of the bulk and backside implant. It is important to note that the electric field in the multiplication layer cannot directly be probed with this method, since the laser beam width is larger than the multiplication implant.

3.5. Sensor capacitance and depletion voltage

Measurements of the capacitance were carried out for every annealing step. In Fig. 9, CV measurements of LGAD W5_I3_1 are shown as an example, the second LGAD shows a similar behavior. The value of the total capacitance decreases after reverse bias is applied, until at 26 V a sharp increase of capacitance is observed. From the local maximum value at about 26 to 30 V the capacitance decreases to a stable value at high bias voltages. This behavior is not observed for the PIN diode and must therefore be related to the presence of the multiplication layer. The increase of the capacitance coincides with the voltage from which on the gain layer seems to be depleted, as can be seen from IV measurements (Fig. 3).

The depletion voltage is obtained by fitting a straight line to the rising slope of the $1/C^2$ values. To avoid the aforementioned increase of the measured capacitance, only values above 30 V bias voltage were included in the fit. The depletion voltage is then the intersection of this line with a horizontal line through the maximum measured capacitance. Due to the more complex shape of the CV curve and the fact that the transition from the rising slope to constant values for $1/C^2$ extends over a large voltage range, a determination of the depletion voltage from these measurements, especially after irradiation, has only limited accuracy. In Fig. 10 the depletion voltage is shown as a function of annealing time for both LGADs. The depletion voltage before irradiation was about 70 V, although edge-TCT measurements show that some charge is collected everywhere in the device already

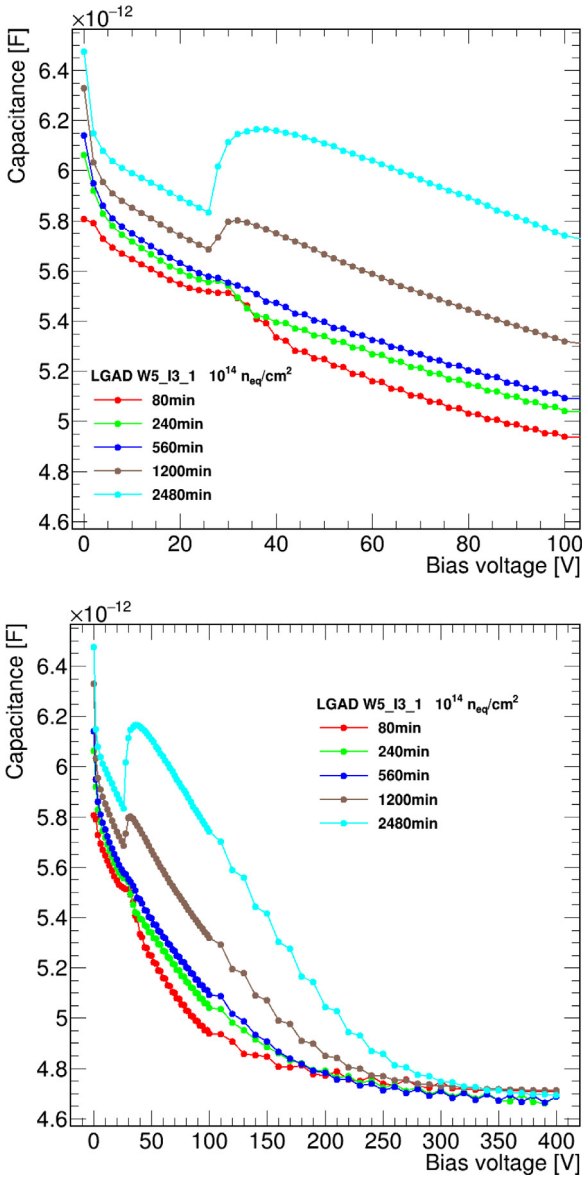

Fig. 9. Capacitance as a function of bias voltage for LGAD W5_I3_1 at different annealing states. CV measurements were carried out at 10 kHz with an alternating voltage amplitude of 0.5 V. The data is shown in a limited voltage range (top) and in the full range (bottom).

at lower voltages of about 35 to 45 V. After irradiation the depletion voltage is increased to 140 V and then rises to values of about 280V after 2480 min of annealing. The PIN diode has a depletion voltage of 40 V before irradiation. After irradiation the depletion voltage increases to about 95 V and rises further to values of about 250 – 300 V with annealing, comparable to the LGADs. The monotonous increase in depletion voltage indicates that the devices are undergoing reverse annealing. The measurement of the sensor W5_E3_1 after 80 min of annealing failed, which was only realized after performing the next annealing step. Therefore one point is missing in the graph.

3.6. Current related damage rate

The current related damage rate α is the change in leakage current after irradiation ΔI, normalized by the neutron equivalent fluence and the active sensor volume V:

$$\alpha = \frac{\Delta I}{\Phi_{eq} \times V} \tag{4}$$

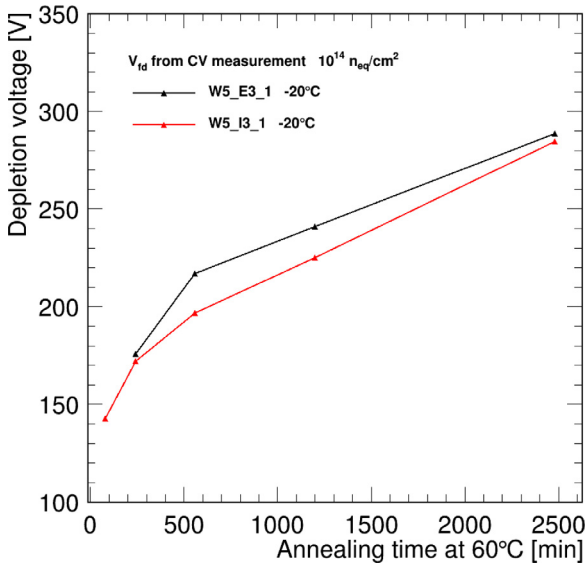

Fig. 10. Depletion voltage as a function of annealing times for both LGADs. The values are obtained from CV measurements.

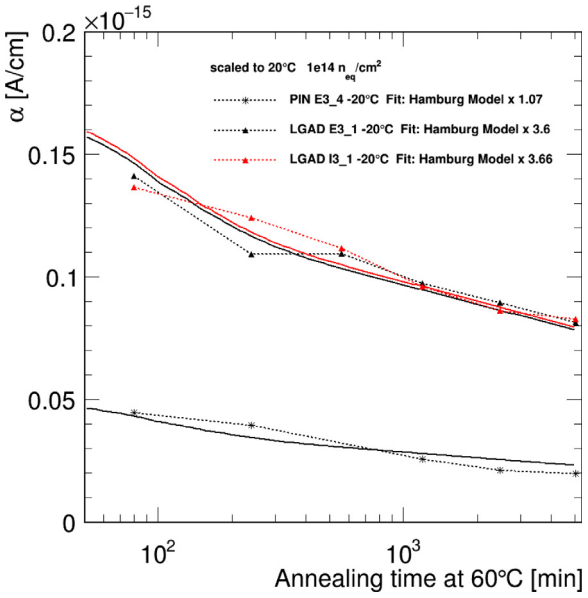

Fig. 11. Current related damage rate as a function of annealing time for both LGADs and the PIN diode. The respective fit by Eq. (5) is shown as a solid line. The measurements were performed at −20 °C and scaled to +20 °C.

The sensor volume is calculated from the geometric properties of the device: $V = 3 \times 3\ \text{mm}^2 \times 277\ \mu\text{m}$. The leakage current before irradiation is much lower and can therefore be neglected in the calculation. The change of α with annealing time t can be parameterized by the equation

$$\alpha(t) = \alpha_1 \cdot \exp\left(\frac{-t}{\tau_1}\right) + \alpha_0 - \alpha_2 \cdot \ln\left(\frac{t}{t_0}\right). \tag{5}$$

A description of the parameters and an interpretation of this equation can be found in [36,37]. This equation does not describe the voltage dependence of the leakage current above full depletion, which is usually observed in measurements of irradiated detectors. Therefore, for each annealing step, a measurement at a bias voltage with a 10–20% margin above the full depletion voltage, ranging from 150 V for 80 min annealing to 400 V for 5040 min annealing, was chosen for the calculation. The used bias voltages are the same across the three devices. The leakage current measurements were carried out without connecting the guard ring. To correct for the difference between the measured total current and the pad current, IV measurements after irradiation and 80 min of annealing, during which the pad and total current were measured separately before mounting the respective sensor on the PCB for TCT measurements, were used. To obtain the α value originating from the pad current, the ratio of total current to pad current was calculated from this measurement. Measurements after annealing were then scaled by this factor. For both LGADs this ratio was 1.41 and proved to be voltage independent. For the PIN a slight voltage dependence was found, ranging from 2.06 (150 V) to 2.28 (400 V). In Fig. 11 the measured current related damage rate is shown as a function of annealing time. Each set of measurements was fitted with Eq. (5) ('Hamburg model'), the only free fit parameter being a constant factor, which is stated in the legend of the figure for each sensor. For the fit, the parameters $t_0 = 1$ min, $\tau_1 = 94$ min, $\alpha_0 = 1.26 \cdot 10^{-17}$ A/cm, $\alpha_1 = 4.87 \cdot 10^{-17}$ A/cm and $\alpha_2 = 3.16 \cdot 10^{-17}$ A/cm are used [37]. In this case, the leakage current measurements were performed at −20 °C and scaled to +20 °C, the annealing was always done at 60 °C. For scaling the leakage current to temperature T the formula

$$I(T) = I(T_0)\left(\frac{T}{T_0}\right)^2 \exp\left[-\frac{E_{eff}}{2k_B} \cdot \left(\frac{1}{T} - \frac{1}{T_0}\right)\right] \tag{6}$$

was used [38]. $I(T_0)$ is the measured leakage current at temperature T_0, k_B is the Boltzmann constant and $E_{eff} = 1.214$ eV. The temperature scaling in this context only serves to make a comparison to the Hamburg model. The true temperature dependence of LGADs is not described by this equation since the impact ionization coefficients are temperature dependent. The measurement of the PIN diode agrees well with the model prediction. Some uncertainty stems from the choice of the bias voltage and from the temperature measurement. The current measurement of the PIN diode after 560 min of annealing was excluded from the calculation, due to an unexpectedly high leakage current, which can result from too short a settling time after cooling down the sensor. It is expected that the results for the LGADs differ from the model prediction by the multiplication factor. Obtained in this way, the multiplication factor is about 3.6 to 3.7 (or 3.4, when taking the PIN diode as a reference), which is in agreement with the gain value of about 3.5 at −20 °C calculated from charge measurements using TCT (cf. Fig. 2). Since trapping of charge carriers does not impact on measurements of the current, the observed multiplication factor of the leakage current can be higher than that of the collected charge. Furthermore, comparing the measurements of the current related damage rate to the predicted annealing behavior, one can see again that LGADs anneal according to the standard theory and no additional annealing contribution resulting from a recovery of gain can be observed.

4. Discussion

The shape of the CV curves, which show an increase of capacitance at 26 V, is not fully understood. The sudden increase of free charge carriers from multiplication can lead to a smaller depleted region around the junction, effectively increasing the measured capacitance. A similar effect, the increase of capacitance of irradiated LGADs at low voltages, was observed in measurements in a different study [39]. The proposed qualitative explanation of this effect is that the irradiated LGAD behaves like a Shockley diode (pnpn): If the sensor bulk behaves like an n-type bulk, due to acceptor removal and trapping of holes, the junction between the multiplication layer and the sensor bulk has opposite polarity compared to both the junction between the n+ implant and the multiplication layer and the junction between the sensor bulk and the backside contact and is thus forward biased. Under certain conditions, this junction can dominate the overall capacitance of the device. With increasing bias voltage, due to the forward polarity, the capacitance increases, which leads to the observed effect.

IV, CV and edge-TCT measurements suggest a gain layer depletion voltage of 26 V and also the signal onset in RF-TCT measurements converges towards this value with increasing annealing time. For shorter annealing times the value of the onset voltage from RF-TCT measurements does not agree with the gain layer depletion voltage observed in leakage current measurements (Fig. 3). Therefore, special care needs to be taken if it is used to infer on properties of the gain layer. The assumption that the onset voltage, measured by TCT, can be unambiguously used to express the space charge in the gain layer is not always valid. Considering only the initial acceptor removal effect and under the assumption that the gain layer depletion voltage is proportional to the average acceptor density in the gain layer, it is possible to approximate the change of gain layer depletion with

$$V_{mr} \approx V_{mr,0} \cdot \exp\left(-c_A \phi_{eq}\right), \tag{7}$$

according to the procedure in [13]. $V_{mr,0}$ is the gain layer depletion voltage before irradiation, c_A the acceptor removal coefficient and ϕ_{eq} the equivalent fluence. Values of the gain layer depletion voltage before and after irradiation of $V_{mr,0} = 32$ V and $V_{mr} = 26$ V and $\phi_{eq} = 10^{14}$ n_{eq}/cm^2, yield a value of $c_A = 2.1 \cdot 10^{-15}$ cm^2, which is slightly higher, but still in agreement with what is reported in literature (cf. [13,40]).

5. Conclusions

Two Low Gain Avalanche Detectors and one PIN diode were irradiated to a fluence of 1×10^{14} n_{eq}/cm^2 using 24 GeV/c-protons and annealed at a temperature of 60 °C in several steps. TCT, edge-TCT, IV and CV measurements were carried out after each annealing step to calculate the gain and the electric field and to investigate the effect of a change of gain layer depletion voltage with irradiation and annealing. It was found that the onset voltage, measured by injecting red laser light to the top side of the device, increases after irradiation and decreases with successive annealing to a lower value than before irradiation. At the same time, by performing edge-TCT measurements after irradiation, an electric field at the backside of the sensors was found. With longer annealing times the field at the backside vanished. IV and CV measurements indicate the depletion of the gain layer at a fixed voltage, independent of annealing time. The value of the onset voltage measured by RF-TCT after long annealing times coincides with the gain layer depletion voltage observed in the leakage current. This leads to the conclusion that the shift to higher values than before irradiation, observed with RF-TCT measurements, is linked to the change of the electric field profile in the sensor bulk rather than a change of the properties of the multiplication layer itself. Care has to be taken when drawing conclusions on the sensor properties only from one type of measurement. Measurements of the leakage current and capacitance, as shown in this study, are an important complement to an analysis of the signal from TCT.

The multiplication layer is affected in such a way that its depletion voltage is reduced after irradiation due to acceptor removal. Measurements of the signal gain as a function of annealing time as well as a comparison of the leakage current to the standard parameterization of annealing show no recovery of gain.

CRediT authorship contribution statement

Moritz Wiehe: Software, Validation, Formal analysis, Investigation, Data curation, Writing - original draft, Writing - review & editing, Visualization, Project administration. **Marcos Fernández García:** Conceptualization, Methodology, Software, Validation, Resources, Data curation, Writing - review & editing, Supervision, Project administration. **Salvador Hidalgo:** Conceptualization, Methodology, Validation, Resources. **Michael Moll:** Conceptualization, Methodology, Software, Validation, Resources, Data curation, Writing - review & editing, Supervision, Project administration, Funding acquisition. **Sofia Otero Ugobono:** Investigation, Writing - review & editing. **Ulrich Parzefall:** Supervision, Funding acquisition. **Giulio Pellegrini:** Conceptualization, Methodology, Validation, Resources. **Ana Ventura Barroso:** Investigation. **Ivan Vila Alvarez:** Conceptualization, Methodology, Validation, Resources, Data curation, Writing - review & editing.

Declaration of competing interest

The authors declare that they have no known competing financial interests or personal relationships that could have appeared to influence the work reported in this paper.

Acknowledgments

This work was performed in the framework of the RD50 collaboration and has been sponsored by the Wolfgang Gentner Programme of the German Federal Ministry of Education and Research (grant no. 05E15CHA).

References

[1] N. Cartiglia, Timing layers 4- and 5-dimension tracking, Nucl. Instrum. Methods Phys. Res. A 924 (2019) 350–354, 11th International Hiroshima Symposium on Development and Application of Semiconductor Tracking Detectors.

[2] G. Pellegrini, M. Baselga, M. Carulla, V. Fadeyev, P. Fernández-Martínez, M. Fernández García, D. Flores, Z. Galloway, C. Gallrapp, S. Hidalgo, Z. Liang, A. Merlos, M. Moll, D. Quirion, H. Sadrozinski, M. Stricker, I. Vila, Recent technological developments on LGAD and iLGAD detectors for tracking and timing applications, Nucl. Instrum. Methods Phys. Res. A 831 (2016) 24–28, Proceedings of the 10th International Hiroshima Symposium on the Development and Application of Semiconductor Tracking Detectors.

[3] H.F.-W. Sadrozinski, S. Ely, V. Fadeyev, Z. Galloway, J. Ngo, C. Parker, B. Petersen, A. Seiden, A. Zatserklyaniy, N. Cartiglia, F. Marchetto, M. Bruzzi, R. Mori, M. Scaringella, A. Vinattieri, Ultra-fast silicon detectors, Nucl. Instrum. Methods Phys. Res. A 730 (2013) 226–231, Proceedings of the 9th International Conference on Radiation Effects on Semiconductor Materials Detectors and Devices.

[4] N. Cartiglia, Design optimization of ultra-fast silicon detectors, Nucl. Instrum. Methods Phys. Res. A 796 (2015) 141–148, Proceedings of the 10th International Conference on Radiation Effects on Semiconductor Materials Detectors and Devices.

[5] M. Centis Vignali, P. Dias De Almeida, L. Franconi, M. Gallinaro, Y. Gurimskaya, B. Harrop, W. Holmkvist, C. Lu, I. Mateu, M. McClish, K.T. McDonald, M. Moll, F.M. Newcomer, S. Otero Ugobono, S. White, M. Wiehe, Deep diffused Avalanche photodiodes for charged particles timing, Nucl. Instrum. Methods Phys. Res. A (2019) 162405.

[6] ATLAS Collaboration, Technical Proposal: A High-Granularity Timing Detector for the ATLAS Phase-II Upgrade, (CERN-LHCC-2018-023. LHCC-P-012), 2018.

[7] CMS Collaboration, Technical Proposal for a MIP Timing Detector in the CMS Experiment Phase 2 Upgrade, 2017.

[8] M. Albrow, M. Arneodo, V. Avati, J. Baechler, N. Cartiglia, M. Deile, M. Gallinaro, J. Hollar, M. Lo Vetere, K. Oesterberg, N. Turini, J. Varela, D. Wright, and Collaboration CMS-TOTEM, CMS-TOTEM Precision Proton Spectrometer, (CERN-LHCC-2014-021. TOTEM-TDR-003. CMS-TDR-13), 2014.

[9] M. Petruzzo, Fast Timing Detector Developments for a LHCb Upgrade-II, Technical report, 2018.

[10] G. Pellegrini, P. Fernández-Martínez, M. Baselga, C. Fleta, D. Flores, V. Greco, S. Hidalgo, I. Mandić, G. Kramberger, D. Quirion, et al., Technology developments and first measurements of Low Gain Avalanche Detectors (LGAD) for high energy physics applications, Nucl. Instrum. Methods Phys. Res. A 765 (2014) 12–16.

[11] I. Tapan, A.R. Duell, R.S. Gilmore, T.J. Llewellyn, S. Nash, R.J. Tapper, Avalanche photodiodes as proportional particle detectors, Nucl. Instrum. Methods Phys. Res. A 388 (1) (1997) 79–90.

[12] V. Greco, G. Pellegrini, C. Gallrapp, V. Fadeyev, S. Hidalgo, J. Lange, D. Flores, S. Grinstein, R. Mori, U. Parzefall, et al., Devices optimised for avalanche multiplication, PoS (2015) 031.

[13] G. Kramberger, M. Baselga, V. Cindro, P. Fernandez-Martinez, D. Flores, Z. Galloway, A. Gorišek, V. Greco, S. Hidalgo, V. Fadeyev, et al., Radiation effects in low gain avalanche detectors after hadron irradiations, J. Instrum. 10 (07) (2015) P07006.

[14] C. Gallrapp, M. Fernández García, S. Hidalgo, I. Mateu, M. Moll, S. Otero Ugobono, G. Pellegrini, Study of gain homogeneity and radiation effects of low gain avalanche pad detectors, Nucl. Instrum. Methods Phys. Res. A 875 (2017) 27–34.

[15] M. Moll, Displacement damage in silicon detectors for high energy physics, IEEE Trans. Nucl. Sci. 65 (8) (2018) 1561–1582.
[16] M. Moll, Acceptor removal - Displacement damage effects involving the shallow acceptor doping of p-type silicon devices, in: The 28th International Workshop on Vertex Detectors - Vertex2019, Lopud, Croatia, 2019.
[17] R. Wunstorf, W.M. Bugg, J. Walter, F.W. Garber, D. Larson, Investigations of donor and acceptor removal and long term annealing in silicon with different boron/phosphorus ratios, Nucl. Instrum. Methods Phys. Res. A 377 (2) (1996) 228–233, Proceedings of the Seventh European Symposium on Semiconductor.
[18] E.M. Donegani, E. Fretwurst, E. Garutti, Defect spectroscopy of proton-irradiated thin p-type silicon sensors, in: 2016 16th European Conference on Radiation and Its Effects on Components and Systems (RADECS), 2016, pp. 1–6.
[19] Y. Gurimskaya, P.D. de Almeida, M. Fernandez Garcia, I. Mateu Suau, M. Moll, E. Fretwurst, L. Makarenko, I. Pintilie, Radiation damage in p-type EPI silicon pad diodes irradiated with protons and neutrons, Nucl. Instrum. Methods Phys. Res. A (2019).
[20] R. Dalal, G. Jain, A. Bhardwaj, K. Ranjan, TCAD simulation of low gain avalanche detectors, Nucl. Instrum. Methods Phys. Res. A 836 (2016) 113–121.
[21] E. Verbitskaya, V. Eremin, A. Zabrodskii, P. Luukka, Simulation of low gain avalanche detector characteristics based on the concept of negative feedback in irradiated silicon detectors with carrier impact ionization, J. Instrum. 11 (12) (2016) P12012.
[22] S. Otero Ugobono, M. Carulla, M. Centis Vignali, M. Fernández García, C. Gallrapp, S. Hidalgo Villena, I. Mateu, M. Moll, G. Pellegrini, I. Vila, Radiation tolerance of proton-irradiated LGADs, IEEE Trans. Nucl. Sci. (2018).
[23] V. Eremin, E. Verbitskaya, Z. Li, The origin of double peak electric field distribution in heavily irradiated silicon detectors, Nucl. Instrum. Methods Phys. Res. A 476 (3) (2002) 556–564, Proc. of the 3rd Int. Conf. on Radiation Effects on Semiconductor Materials, Detectors and Devices.
[24] G. Kramberger, V. Cindro, I. Mandić, M. Mikuž, M. Zavrtanik, Field engineering by continuous hole injection in silicon detectors irradiated with neutrons, Nucl. Instrum. Methods Phys. Res. A 497 (2) (2003) 440–449.
[25] V. Eremin, N. Strokan, E. Verbitskaya, Z. Li, Development of transient current and charge techniques for the measurement of effective net concentration of ionized charges (N_{eff}) in the space charge region of p–n junction detectors, Nucl. Instrum. Methods Phys. Res. A 372 (3) (1996) 388–398.
[26] Centre Nacional de Microelectrònica, IMB-CNM-CSIC, Barcelona, Spain, 2018.
[27] PS IRRAD Proton Facility, CERN, 2018.
[28] I. Mateu, M. Moll, F. Ravotti, M. Glaser, H. Neugebauer, E. Curras, NIEL hardness factor determination for the new proton irradiation facility at CERN, 2016.
[29] C. Gallrapp, et al., The TCT+ Setup - a System for TCT, ETCT and Timing Measurements. Presented at the 1st TCT Workshop, DESY, Hamburg, Germany, 2015.
[30] R. Mulargia, R. Arcidiacono, A. Bellora, M. Boscardin, N. Cartiglia, F. Cenna, R. Cirio, G.F. Dalla Betta, S. Durando, A. Fadavi, et al., Temperature dependence of the response of ultra fast silicon detectors, in: International Workshop on Semiconductor Pixel Detectors for Particles and Imaging (Pixel 2016), 2016, pp. 1–8.
[31] G. Kramberger, M. Carulla, E. Cavallaro, V. Cindro, D. Flores, Z. Galloway, S. Grinstein, S. Hidalgo, V. Fadeyev, J. Lange, et al., Radiation hardness of thin low gain avalanche detectors, Nucl. Instrum. Methods Phys. Res. A 891 (2018) 68–77.
[32] M. Ferrero, O.H. Ali, R. Arcidiacono, M. Boscardin, N. Cartiglia, F. Cenna, R. Cirio, M. Costa, G.F. Dalla Betta, F. Ficorella, S. Giordanengo, M. Mandurrino, V. Monaco, M.M. Obertino, L. Pancheri, G. Paternoster, R. Sacchi, F. Siviero, V. Sola, A. Staian, A. Vignati, Developments in the FBK production of ultra -fast silicon detectors, 2017.
[33] M. Shur, 6 - Semiconductors, in: WAI-KAI CHEN, Editor, in: The Electrical Engineering Handbook, Academic Press, Burlington, 2005, pp. 153–162.
[34] W. Maes, K. De Meyer, R. Van Overstraeten, Impact ionization in silicon: A review and update, Solid-State Electron. 33 (6) (1990) 705–718.
[35] G. Kramberger, Signal Development in Irradiated Silicon Detectors (Ph.D. thesis), Stefan Inst., Ljubljana, 2001.
[36] M. Moll, Radiation Damage in Silicon Particle Detectors: Microscopic Defects and Macroscopic Properties, Technical report, DESY, 1999.
[37] M. Moll, E. Fretwurst, M. Kuhnke, G. Lindström, Relation between microscopic defects and macroscopic changes in silicon detector properties after hadron irradiation, Nucl. Instrum. Methods Phys. Res. B 186 (1) (2002) 100–110.
[38] A. Chilingarov, Temperature dependence of the current generated in Si bulk, J. Instrum. 8 (10) (2013) P10003.
[39] I. Vila Alvarez, Instituto de Física de Cantabria (CSIC-UC), Radiation tolerance of thin LGAD detectors and in-depth study of ILGAD timing performance, in: 14th Trento Workshop on Advanced Silicon Radiation Detectors, 2019.
[40] M. Ferrero, R. Arcidiacono, M. Barozzi, M. Boscardin, N. Cartiglia, G.F. Dalla Betta, Z. Galloway, M. Mandurrino, S. Mazza, G. Paternoster, F. Ficorella, L. Pancheri, H.-F.W. Sadrozinski, F. Siviero, V. Sola, A. Staiano, A. Seiden, M. Tornago, Y. Zhao, Radiation resistant LGAD design, Nucl. Instrum. Methods Phys. Res. A 919 (2019) 16–26.